Detecting bifurcations in 2D periodic metamaterials from images

M. Poncelet
Université Paris-Saclay, CentraleSupélec, ENS Paris-Saclay, CNRS LMPS - Laboratoire de Mécanique Paris-Saclay, 91190 Gif-sur-Yvette, France

C. Combescure
Saint-Cyr Coetquidan Military Academy, CReC Saint-Cyr, 56380 Guer, France University Bretagne Sud, UMR CNRS 6027, IRDL, F-56100 Lorient, France

F. Amiot*
Université de Franche-Comté, CNRS, FEMTO-ST Institute, F-25030 Besançon, France
Tel.: +33-3-81666014 fabien.amiot@femto-st.fr

Abstract

Architectured materials are often used for their high strength-to-weight ratio. For this matter, they are designed with high porosity which makes them sensitive to buckling under compressive loading. This buckling is usually predicted by numerical computations but very few experiments are available to confront these numerical results. Experimentally, the onset of instabilities is usually determined by following the global force applied onto the sample. However, this detection might be hindered by the presence of various defects which may locally trigger the instabilities. A very simple technique is proposed herein to detect instabilities in periodic architectured materials using standard imaging techniques. It is shown to be applicable at a local scale, thereby allowing for a local instability detection.

Keywords: Metamaterials, Instabilities, Imaging

1. Introduction

Architectured materials are composite materials in which the macroscopic properties emerge from the local organisation of constitutive materials in space at the mesoscopic scale. When optimised to improve the stiffness-to-weight ratio, buckling at the mesoscopic scale becomes a possible mode of deformation of these materials [1]. While many studies are focused on the numerical prediction of this buckling [2, 3, 4], there are fewer experimental studies available to validate these numerical results [1, 5]. The comparison criterion between numerical and experimental results is the onset of instability [6] traditionally identified using the global loading force maximum. However, this detection might be hindered, experimentally, by various defects in real systems which may locally trigger the instabilities [1].

The use of full-field kinematic measurements — e.g. Digital Image Correlation (DIC) — for architectured materials is not new. Different techniques have been developed to consider the fact that a large portion of the observed area is void and hence doesn't contain kinematic information. For DIC, one may circumvent the problem by adding a stiffness-free matter [7], use multiscale approaches [8, 9], choose relevant element types (like beam in the case of lattice materials [10]), use high resolution cameras and a mesh based on the mesoarchitecture [11], etc. However all these techniques while providing many information, require non-negligible expertise and do not detect buckling, thus implying further data-processing. This contribution focuses on a simpler way to exploit images to detect buckling.

2. Materials and methods

2.1. Material

The specimen is a parallelepiped rectangle of hexagonal honeycomb, containing 11 × 11 8-mm-diameter holes, with 2-mm menisci. The complete specimen is 111 × 105 mm^2. The out-of-plane thickness (24 mm) prevents global out-of-plane buckling.

The constitutive material is a low stiffness silicon rubber (*Smooth-SilTM 950* by *Smooth-On*, initial tangent Young modulus of 1.9 MPa), displaying high elongation at break (320%) and very low viscosity. The specimen is cast in a 3d-printed mold. This technique enables an accurate geometry of the specimen, offers a wider range of material properties and ensures an extremely low porosity of the constitutive material.

2.2. Biaxial loading and imaging

Bicompaction tests are performed with a machine following the principle proposed by [12] offering the advantage of continuous boundary conditions by use of flat platens contrary to [13] which rely on slotted platens. It also allows different strain ratios, i.e. both uniaxial and equibiaxial loadings.

The setup (Fig. 1) is instrumented with 8 load sensors to assess the force applied by each platens. The measured normal and tangential loadings are globally denoted as $T(s, n)$, with s spanning the $\{1…8\}$ range, and n denoting the image index. In order to describe the loading through a unique scalar, the results are displayed as a function of a global loading parameter $g(n)$ defined such that $T(s, n) \simeq g(n) \times f(s)$. This decomposition is obtained as the leading term of the singular value decomposition (SVD) of $T(s,n)$ [14].

Displacement-controlled equibiaxial compression tests are done at a constant velocity and thus constant macroscopic strain rate (typically below 0.1 %/s). The images $P(x,y,n)$ are obtained with a Digital Single Lens Reflex camera (*70D*, *Canon*) equipped with a 60-mm fixed focal lens (*Canon*), and are 3648 × 5472 pixels in size. x and y denote the position in the image's plane.

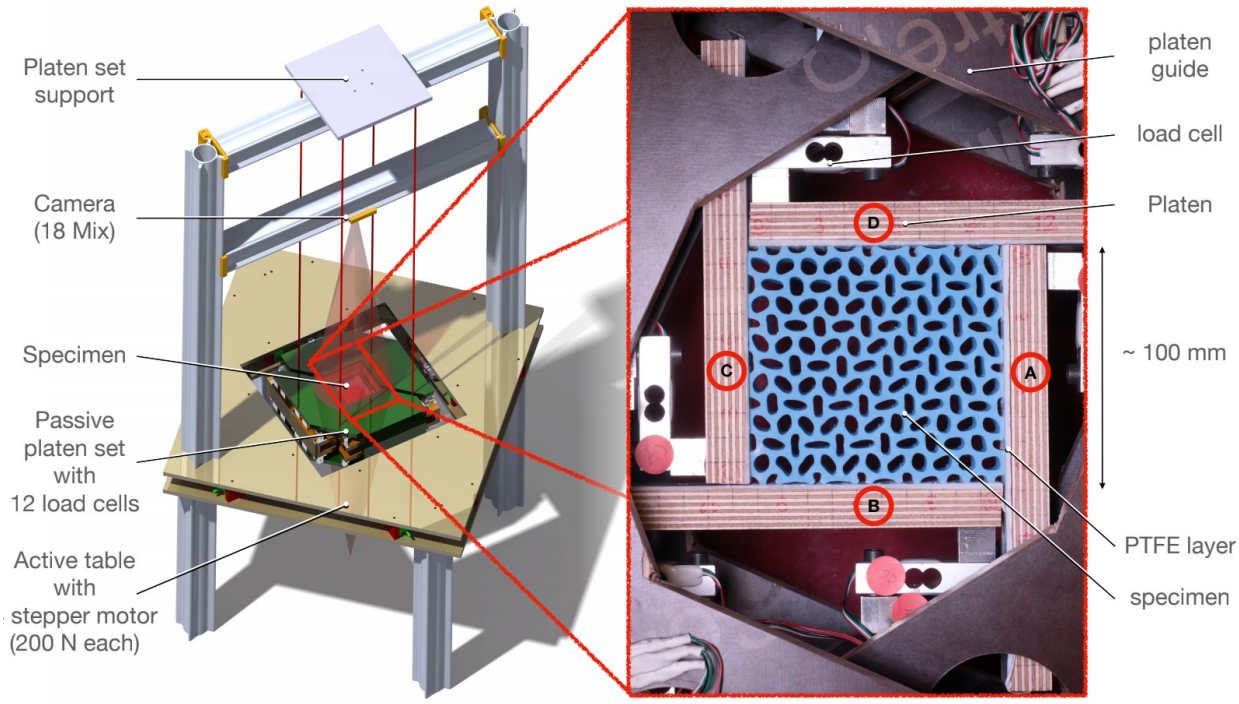

Figure 1: Experimental setup: testing machine (the wires holding the machine horizontally are in dark red) (left) and field of view of the camera (right).

3. Proposed image processing

A region of interest (ROI) $\hat{P}(x,y,n)$ covering the whole sample is defined out of the images $P(x,y,n)$ and windowed. Its boundaries are updated using the measured platens displacements, thus compensating for uniform strains. The Fourier transform $\widetilde{P}(\xi,\eta,n)$ of $\hat{P}(x,y,n)$ reads

$$\widetilde{P}(\xi,\eta,n)=\int \hat{P}(x,y,n)\exp\left(-2i\pi(x\xi+y\eta)\right)dxdy \qquad (1)$$

$\widetilde{P}$ is computed using a fast Fourier transform (FFT). As $\hat{P}$ is real-valued, $\left\|\widetilde{P}(\xi,\eta,n)\right\|$ is symmetric with respect to the ξ and η axes, so that only one quarter of the spectrum is displayed in the following.

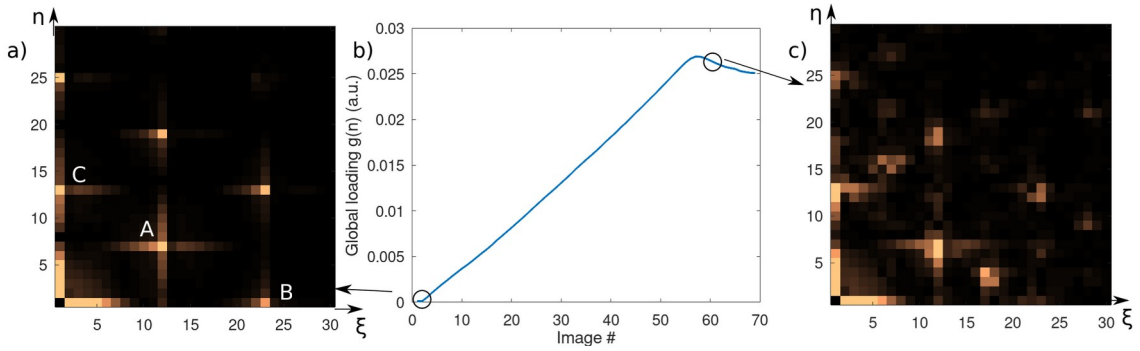

Figure 2: Magnitude of the Fourier spectra of the ROI in the undeformed state $\left\|\widetilde{P}(\xi,\eta,n=1)\right\|$ (left) and after bifurcation $\left\|\widetilde{P}(\xi,\eta,n=61)\right\|$ (right), see the global loading parameter *g(n)* (center).

As presented in Fig. 2 (left), $\left\|\widetilde{P}(\xi,\eta,n=1)\right\|$ displays a well defined structure corresponding to the symmetry of the material in its initial configuration. Indeed, since the initial undeformed geometry of the sample is composed of hexagonal tiling of circular holes, the hexagonal symmetry can be observed on the plot of the Fourier spectra magnitude. For instance, the two peaks *A* and *C* are separated by a 60° angle with respect to the origin. A global loading force maximum is observed at a time corresponding to image *n=57*, indicating the onset of the structural instability (Fig. 2, center). As can be seen from Fig. 2 (right), the magnitude of Fourier spectra obtained for the bifurcated structure shortly after that global loading force maximum (image *n=61*) displays additional, somehow blurry, peaks (see for instance the peak located around (17,3)). Indeed, generic bifurcation breaks symmetry [15] and this symmetry breaking would result in a different arrangement of the peaks in the Fourier transform.

It is therefore proposed to track the instabilities of the structure by defining the indicator $I_{AB}(n)$ such that

$$I_{AB}(n)=\frac{\int_{AB}\left\|\widetilde{P}(\xi,\eta,n)\right\|d\xi\,d\eta}{\left\|\widetilde{P}(A,n)\right\|+\left\|\widetilde{P}(B,n)\right\|} \qquad (2)$$

$I_{AB}(n)$ refers to the rectangular spectral domain *AB*, delimited by the user-defined peaks *A* and *B* (see Fig. 2). This spectral region has to be initially free of any peak and is thus denoted as an empty spectral region (ESR). The indicator (2) thus depends on both the chosen ROI and ESR, and any other ESR, corresponding to any other bifurcated state, could be chosen in Fig 2a.

4. Results

The proposed analysis is first exemplified using a ROI which extends over the full sample for validation purpose. The detected buckling is then said global. The analysis is then performed using ROIs which cover only part of the sample, thus experimentally defining local buckling.

4.1. At the global scale

The indicator I_{AB} defined by Eq. 2 is computed for the ESR delimited by the two peaks *A* and *B* indicated on Fig. 2 (left), and for a ROI covering the full sample. It measures the visibility of a peak appearing in the ESR.

This indicator is displayed together with the global loading parameter as a function of the image index in Fig. 3.

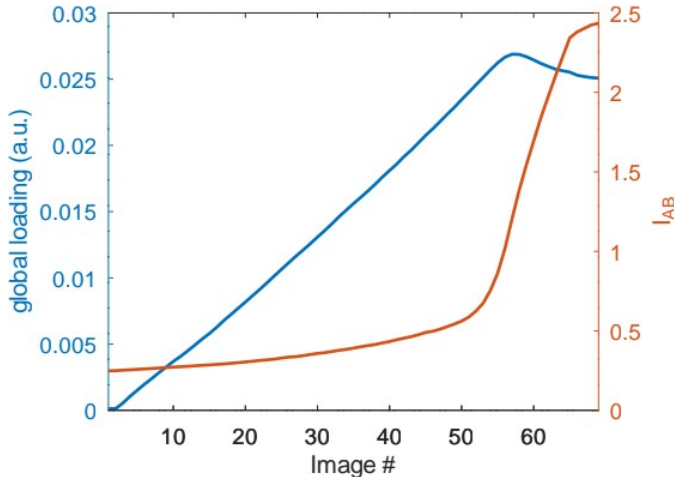

Figure 3: Global bifurcation indicator for the *AB* zone $I_{AB}(n)$ and the global loading parameter $g(n)$ as a function of the image index n.

4.2. At local scale

The initial ROI is divided into 3 × 3 equal, non-overlapping sub-regions. The same computations have been performed independently considering the individual sub-regions as ROIs and keeping the same AB domain as ESR. The resulting indicators are denoted as local in the following.

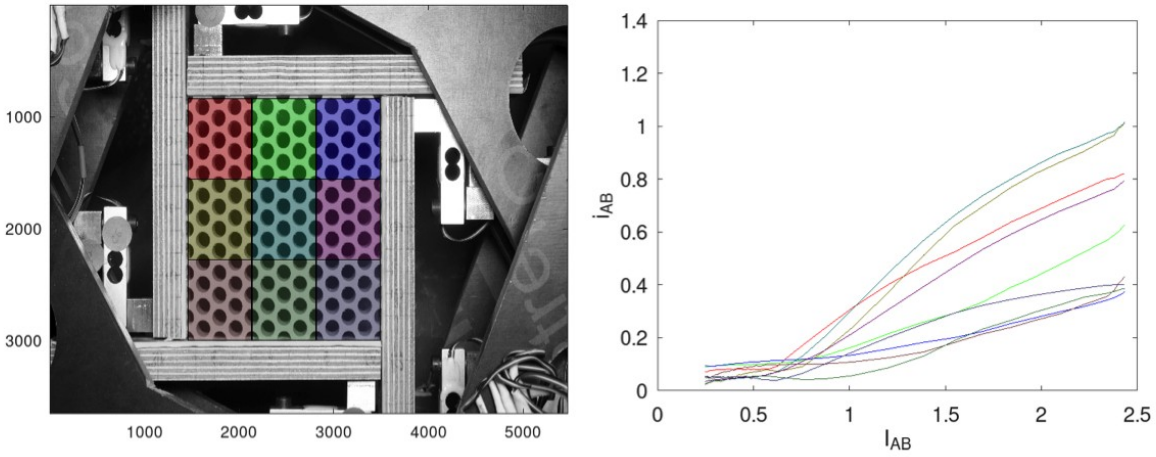

Figure 4: Localization of the nine sub regions (left) and local bifurcation indicator for AB zone $i_{AB}(n)$ as a function of the corresponding global bifurcation indicator $I_{AB}(n)$ (right).

Fig. 4 displays the local indicator $i_{AB}(n)$ computed on the 9 sub-regions as a function of the global indicator $I_{AB}(n)$. Each line corresponds to a particular sub-region, and they share the same color in Fig.4.

5. Discussion

The I_{AB} indicator remains almost constant throughout the specimen loading and suddenly increases when approaching the instability, as it is detected from the global loading maximum. The excellent agreement between the two indicators validates the proposed image-based

indicator for the detection of the onset of instabilities in periodic architectured materials. It should further be highlighted that the detection of the instability via the global loading parameter *g(n)* corresponds to the maximum rate of I_{AB} with respect to the applied strain (around $I_{AB} \simeq 1$).

Fig. 4 further clearly shows that buckling does not appear in a uniform manner across the sample. The local bifurcation indicator clearly increases from $I_{AB} \simeq 0.6$, well before the global instability is detected. This demonstrates the need for such a local bifurcation indicator: it allows to resolve, both in time and space, the transition to the bifurcated state. It further allows to discriminate buckling initiation (as detected by the local indicator) from the global (catastrophic) buckling of the structure.

6. Conclusion

The proposed technique, based on an image processing indicator, has been validated with respect to classical global loading maximum criterion. This image processing technique making only use of FFT, it is simply coded and computationally efficient [16]. As a consequence, it could be used to provide feedback to the machine. It can also provide additional information on a possible non-uniform or premature buckling in the specimen that would not necessarily lead to a drastic change in the global loading indicator. Used as such or combined with a global loading measurement, our proposed technique is a new tool to better understand the local-to-global buckling transition in architectured materials.

Acknowledgements

This work (M.P., C.C.) benefited from the research project ANR-19-CE08-0005 (project Max-Oasis) funded by the French National Research Agency (ANR).

References

[1] Papka, S. D. and Kyriakides, S. ”Biaxial crushing of honeycombs: - Part 1: Experiments.” Int. J. Solids Struct. 36 (1999), 4367–4396.
[2] Triantafyllidis, N. and Schraad, M. W. ”Onset of failure in aluminum honeycombs under general in-plane loading”. J. Mech. Phys. Solids 46 (1998), 1089–1124.
[3] Ohno, N. et al. ”Microscopic symmetric bifurcation condition of cellular solids based on a homogenization theory of finite deformation.” J. Mech. Phys. Solids 50 (2002), 1125–1153.
[4] Saiki, I., et al. ”Flower patterns appearing on a honeycomb structure and their bifurcation mechanism.” Int. J. Bifurc. Chaos 15 (2005), 497–515.
[5] Scarpa, F., et al. ”Elastic buckling of hexagonal chiral cell honeycombs.” Composites Part A: Applied Science and Manufacturing 38.2 (2007): 280-289.
[6] Combescure, C., et al. ”Deformation Patterns and their Stability in Finitely Strained Circular Cell Honeycombs.” J. Mech. Phys. Solids 142 (2020), 103976.
[7] Poncelet, M. et al. ”An experimental evidence of the failure of Cauchy elasticity for the overall modeling of a non-centro- symmetric lattice under static loading” Int. J. Solids Struct. 147 (2018): 223-237
[8] Agnelli, F. et al. ”Systematic two-scale image analysis of extreme deformations in soft architectured sheets”, Int. J. Mech. Sc. 194 (2021) 106205.
[9] Hild, F. et al. ”Multiscale DIC applied to Pantographic Structures”, Exp. Mech. 61 (2021) 431-443

[10] Somera, A. ”On the effective elasticity of quasi-periodic lattice materials : From microscopic foundations to experimental validation”, PhD thesis, Ecole centrale de Nantes (2022)
[11] Rouwane, A. et al. ”Architecture-Driven Digital Image Correlation Technique (ADDICT) for the measurement of sub-cellular kinematic fields in speckle-free cellular materials” Int. J. Solids Struct. 234–235 (2022) 111223
[12] Hambly E. C. ”A new true triaxial apparatus” Geotechnique 19 2 (1969): 307-309.
[13] Shan, S. et al. ”Harnessing multiple folding mechanisms in soft periodic structures for tunable control of elastic waves.” Advanced Functional Materials 24.31 (2014): 4935-4942.
[14] Press W.H. et al. “Numerical recipes in C++”, Cambridge University Press (2002).
[15] Sattinger, D. H. Group Theoretic Methods in Bifurcation Theory. vol. 762 (Springer Berlin Heidelberg, 1979).
[16] IBIS : doi:10.5281/zenodo.8252796